



**HAL**  
open science

# Measurement of the Influence of the Microstructure of Alumina-Supported Cobalt Catalysts on their Activity and Selectivity in Fischer-Tropsch Synthesis by using Steady-State and Transient Kinetics

Edouard Rebmann, Pascal Fongarland, Vincent Lecocq, Fabrice Diehl, Yves Schuurman

## ► To cite this version:

Edouard Rebmann, Pascal Fongarland, Vincent Lecocq, Fabrice Diehl, Yves Schuurman. Measurement of the Influence of the Microstructure of Alumina-Supported Cobalt Catalysts on their Activity and Selectivity in Fischer-Tropsch Synthesis by using Steady-State and Transient Kinetics. *Chem-CatChem*, 2017, 9 (12), pp.2344 - 2351. 10.1002/cctc.201700078 . hal-01582167

**HAL Id: hal-01582167**

**<https://ifp.hal.science/hal-01582167>**

Submitted on 3 May 2021

**HAL** is a multi-disciplinary open access archive for the deposit and dissemination of scientific research documents, whether they are published or not. The documents may come from teaching and research institutions in France or abroad, or from public or private research centers.

L'archive ouverte pluridisciplinaire **HAL**, est destinée au dépôt et à la diffusion de documents scientifiques de niveau recherche, publiés ou non, émanant des établissements d'enseignement et de recherche français ou étrangers, des laboratoires publics ou privés.

# Influence of microstructure of Co/Al<sub>2</sub>O<sub>3</sub> catalysts on activity and selectivity in Fischer-Tropsch synthesis by steady-state and transient kinetics

E. Rebmann<sup>[b]</sup>, P. Fongarland<sup>[a]</sup>, V. Lecocq<sup>[b]</sup>, F. Diehl<sup>[b]</sup>, and Y. Schuurman <sup>\*[a]</sup>

**Abstract:** Five alumina supported cobalt catalysts with different particle size and structure were synthesized. The catalysts showed different activities during long-term Fischer-Tropsch experiments. SSITKA <sup>12</sup>CO/H<sub>2</sub> => <sup>13</sup>CO/H<sub>2</sub> experiments were carried out during these long-term runs. The number of active sites for CO adsorption and activation was estimated through the summation of all surface intermediates derived from SSITKA experiments. Rather than comparing Turnover Frequencies (TOF), a kinetic analysis was performed. A simple kinetic rate equation based on the *in-situ* number of active sites described adequately the steady-state CO conversion over the 5 catalysts. Thus the difference in the catalytic performance could not be attributed to a difference in particle size, phase orientation (fcc or hcp) or Pt promoting effect, but instead was only due to the number of reduced cobalt atoms exposed during reaction. Similarly, the selectivity depended on the CO conversion level and temperature, but not on the catalyst structure.

## Introduction

Fischer-Tropsch synthesis (FTS) is expected to become an important process for the conversion of biomass into liquid transport fuels. FTS converts syngas (a mixture of carbon monoxide and hydrogen) into long chain hydrocarbons. Currently syngas for FTS is obtained from coal and natural gas, but syngas production from 2<sup>nd</sup> generation biomass and waste has been demonstrated on pilot scale level and a Biomass-to-Liquids (BTL) demonstrator has been started recently in northern France <sup>[1]</sup>. Both iron and cobalt based catalysts are used for FTS. Cobalt based catalysts are preferred as they are more active at low temperature, exhibit a higher chain growth probability and do not favor the water-gas shift reaction. Still improvement of the activity and selectivity is highly desirable. Numerous studies have been devoted in understanding the effect of the support and cobalt structure on the catalytic performance <sup>[2-15]</sup>. The precise influence of the catalyst variables remains unclear. The effect of the cobalt particle size on the activity and selectivity are still being debated.

A consensus exists on the turnover frequency over large (> 8 nm) cobalt particles <sup>[10]</sup>. The results diverge over smaller Co particles where some research groups have reported a decrease of the TOF with decreasing particle size <sup>[6,7,9,14]</sup>, while other do not observe this effect <sup>[3,4,12,13]</sup>. The cause for this discrepancy has been attributed to a large range of phenomena such as a preferential oxidation or carbidisation of small cobalt particles, difference in reducibility, formation of cobalt support mixed compounds or to an inappropriate measurement of the surface cobalt atoms. For the latter issue, Yang et al. have recently compared H<sub>2</sub> and CO chemisorption methods to determine the cobalt particle size <sup>[16]</sup>. The data were scattered when plotted versus the H<sub>2</sub> chemisorption results, but better correlations were obtained as a function of the CO chemisorption results. Barbier et al. have also criticized the use of H<sub>2</sub> chemisorption to determine the cobalt particle size <sup>[6]</sup>. Most studies on the cobalt particle size effect have been performed over "model" supports, such as carbon nanofibers or silica, which allow a good reducibility of small cobalt particles. A more industrial support, alumina, has been used in a study by Holmen and coll., who did not find any effect of the particle size on the site-time yield, but found an optimum for the C<sub>5+</sub> selectivity <sup>[11,12]</sup>. On the other hand, Claeys and coll. found that both the activity and selectivity depended on the Co particle size between 2-10 nm <sup>[14]</sup>. In a recent study they stressed the particle-size dependent role of water on the activity, selectivity and stability of alumina supported cobalt catalysts <sup>[15]</sup>. The measurement of the turnover frequency of the FTS over cobalt supported catalysts is not trivial. Besides the phenomena mentioned above, the catalyst needs to be "stabilized" or "conditioned" during several days under syngas partial pressure and mild FT conditions. During this time generally the activity drops and important surface reconstruction takes place, as well as possible carbon formation, oxidation and sintering <sup>[17, 18,19]</sup>. At this point the number of exposed cobalt atoms is generally unknown and the TOF is calculated based on the initial number of active sites. Carvalho et al.<sup>[19]</sup> showed that the deactivation affects the CO adsorption and CH<sub>x</sub> hydrogenation sites differently, rendering the estimation of the TOF more ambiguous. Moreover, the TOF is not an intrinsic catalyst descriptor but it depends on the reaction conditions, such as temperature, pressure and conversion <sup>[20]</sup>. In this study we have investigated a series of alumina support cobalt catalysts with different structures that can be considered as "model" industrial catalysts. Although Steady-State Isotopic Transient Kinetic Analysis (SSITKA) is performed at low pressure, several studies have shown that it gives relevant information on the FTS. Breejen et al.<sup>[9]</sup> used SSITKA to investigate the Co particle size effect and found similar results as those obtained before at 35 bar <sup>[7]</sup>. Van Dijk et al. <sup>[21]</sup> successfully used their SSITKA model to predict the product distribution under

[a] Prof. P. Fongarland and Dr. Y. Schuurman  
IRCELYON, UMR 5256  
CNRS, Université Lyon 1  
2 avenue Albert Einstein, 69626 Villeurbanne Cedex, France  
E-mail: [yves.schuurman@ircelyon.univ-lyon1.fr](mailto:yves.schuurman@ircelyon.univ-lyon1.fr)

[b] Dr. E. Rebmann, Dr. V. Lecocq, Dr. F. Diehl  
IFP Energies nouvelles  
Rond point de l'échangeur de Solaize, BP3, 69360 Solaize, France

Supporting information for this article is given via a link at the end of the document.

industrial conditions. By applying SSITKA during the long-term testing, the number of active sites could be determined *in-situ*. Furthermore, the data are fitted to a kinetic rate equation to report the rate constant for each sample rather than the TOF.

## Results and Discussion

### Catalyst characterization

Table 1 summarizes the main features of the synthesized alumina supported Co catalysts. All samples have similar cobalt content between 13.2-13.3 wt.%. Similar Pt content for the promoted samples was achieved as well. The samples have different cobalt particle sizes as aimed for. XRD analysis and electron microscopy gave different values for the cobalt particle size (even when corrected for the difference between oxide and metal particles), but the general trend is consistent. The cobalt particle size distributions by TEM are rather large, as shown in Figure S3. Jean-Marie<sup>[22]</sup> also observed a larger XRD particle size than TEM or a series of cobalt catalysts on a similar puralox  $\gamma$ -alumina support. He attributed this to the weak contrast of the cobalt oxide under TEM observation, leading to an underestimation of the particle size. The last column of Table 1 lists the number of reduced cobalt surface sites as determined by dynamic CO adsorption. The dynamic CO adsorption only addresses the reduced cobalt surface sites, as the reversible adsorption was discarded in the calculation of the number of sites. The reversible CO adsorption corresponds to the part of the cobalt that is still oxidized even after the hydrogen reduction treatment. From previous studies<sup>[23,24]</sup>, a degree of reduction is expected for the non-promoted and Pt promoted samples of 60-70% and 75-90%, respectively. Moreover, the larger cobalt particles will have a higher degree of reduction than the small ones.

The specific surface area of the alumina support was decreased from 166 m<sup>2</sup>/g to approximately 135 m<sup>2</sup>/g. The mean pore diameter was for all samples 9.5  $\pm$  0.5 nm.

### CO conversion over Co/Al<sub>2</sub>O<sub>3</sub> catalysts

Figure 1 shows the CO conversion as a function of time on stream (TOS) for the 5 tested catalysts. To evaluate the repeatability of the experiments, two series of replicates with the same catalyst (2 tests with Co/Al<sub>2</sub>O<sub>3</sub>-10nm fcc) under the same conditions at three different temperatures were performed. An excellent reproducibility was obtained for both the activity and the selectivity, as reported in the supporting information. Based on the average values and on the variance, it appeared that the relative errors of the measured conversions and selectivity were lower than 5% for TOS > 3h.

For all 5 tests, initially a sharp decrease of the CO conversion is observed during the first 3 hours, followed by a much slower decrease of the CO conversion as a function of time. Towards the end of the catalytic tests, the reactor temperature has been changed resulting in sudden changes of the CO conversion, as shown in Figure 1 in the top part. For some samples the H<sub>2</sub>/CO ratio has also been varied between values in the range of 2 - 10.

**Table 1.** Summary of the catalyst properties.  $d_{\text{XRD}}$  and  $d_{\text{va}}$  derived from XRD and electron microscopy, respectively.  $N_{\text{s}}^{\circ}$  are quantified by dynamic CO adsorption before the long-term testing.

Catalyst	wt.% Co	ppm Pt	$d_{\text{XRD}}$ (Co <sub>3</sub> O <sub>4</sub> ) nm	$d_{\text{va}}$ (Co <sup>0</sup> ) nm	$N_{\text{s}}^{\circ}$ mmol/kg <sub>cat</sub>
CoPt/Al <sub>2</sub> O <sub>3</sub> -6nm	13.2	360	6	6.5 $\pm$ 2.7	108
CoPt/Al <sub>2</sub> O <sub>3</sub> -10nm	13.2	340	10	7.6 $\pm$ 2.8	91
CoPt/Al <sub>2</sub> O <sub>3</sub> -15nm	13.2	355	15	10.4 $\pm$ 4.5	67
Co/Al <sub>2</sub> O <sub>3</sub> -10nm (fcc)	13.3	0	10	7.6 $\pm$ 2.7	103
Co/Al <sub>2</sub> O <sub>3</sub> -10nm (hcp)	13.3	0			63

[a] Table Footnote. [b] ...

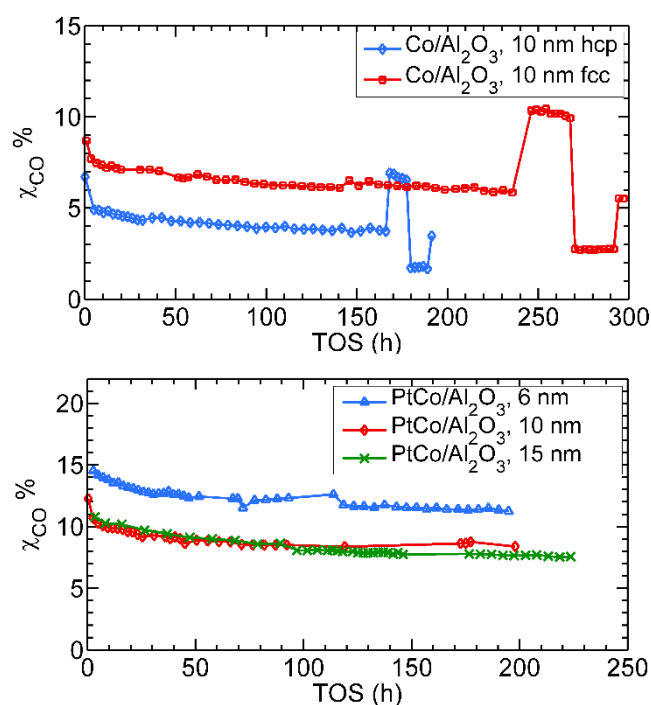


**Figure 1.** CO conversion with TOS for the 5 catalyst samples. Starting conditions: 220°C for hcp and fcc Co/ Al<sub>2</sub>O<sub>3</sub> 10 nm catalysts, 225°C for CoPt/ Al<sub>2</sub>O<sub>3</sub> 6,10,15 nm catalysts. H<sub>2</sub>/CO=2, 300 mg catalyst.

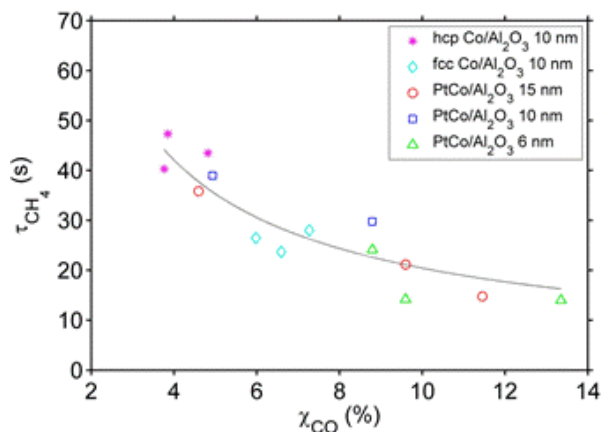


**Figure 2.** The surface lifetime of the intermediates leading to methane as a function of the CO conversion for all 5 catalysts at 215, 225 & 235°C.

During these long-term tests several SSITKA  $^{12}\text{CO}/\text{H}_2 \Rightarrow ^{13}\text{CO}/\text{H}_2$  switches have been performed. The SSITKA experiment lasted approximately 10 minutes and are therefore representative for a catalyst performance at a given TOS. These SSITKA experiments provide more detailed kinetic information and have also been used to calculate the number of active sites during TOS. A typical SSITKA responses of Kr, CO and the fully labeled  $^{13}\text{C}$  hydrocarbons up to  $\text{C}_4$ , after a  $^{12}\text{CO}/^{13}\text{CO}$  switch over the fcc  $\text{Co}/\text{Al}_2\text{O}_3$  at 220°C after 150 h of TOS, has been reported in [24].

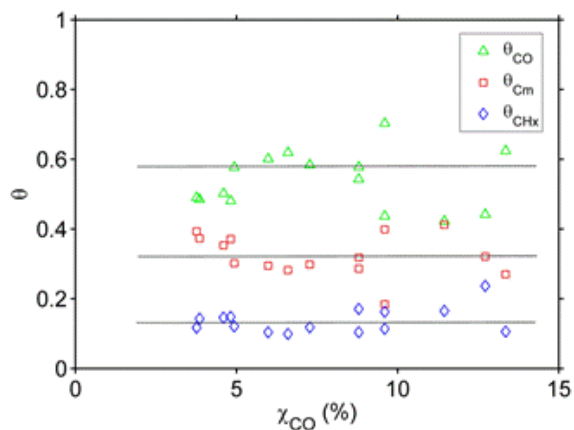


**Figure 3.** The surface coverages of adsorbed CO, the monomeric carbon species,  $\text{C}_m$ , and the  $\text{CH}_x$  species as a function of the CO conversion for all 5 catalysts at 215, 225 & 235°C.

Figure 2 shows the surface lifetime of the intermediates leading to methane as a function of the CO conversion for all 5 catalysts at three reaction temperatures. The observed trend suggests that

the methane surface lifetime is governed by the conversion rather than the temperature or catalysts structure. A similar result was obtained for the intermediates leading to  $\text{C}_{2+}$  (Fig. 4S). In order to estimate the total number of active sites from the SSITKA data, three carbon containing intermediates were identified and quantified. Previous studies [21] proposed a scheme based on a  $\text{CH}_x^*$  reservoir between the adsorbed CO and the methane or the surface growing intermediate species. Here an additional intermediate, the monomeric carbon species involved in the propagation step has been used for the analysis of the transient data. This scheme better reflects the Fischer-Tropsch conditions, where the  $\text{C}_5+$  selectivity is significant, compared to the previous scheme that was used mainly under methanation conditions (high  $\text{H}_2/\text{CO}$  ratios). Figure 3 plots the surface coverages of adsorbed CO, the monomeric carbon species and the  $\text{CH}_x$  species for the 5 catalyst samples at the three reaction temperatures as a function of the conversion. Like for the surface lifetime, trends as a function of the conversion are observed, rather than effects of catalyst structure or reaction temperature. The CO,  $\text{CH}_x$  and  $\text{C}_m$  coverages are constant for all investigated conversions.

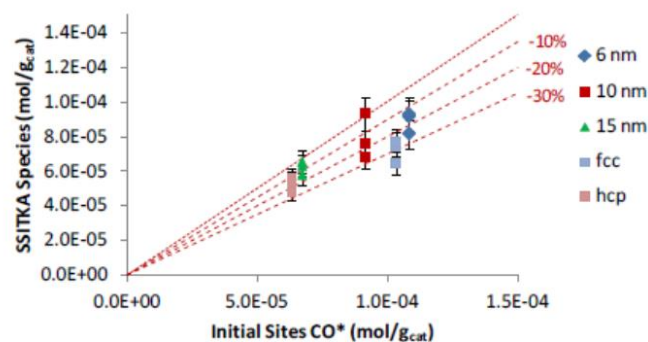


**Figure 4.** The summation of the surface coverages of adsorbed CO, the monomeric carbon species,  $\text{C}_m$ , and the  $\text{CH}_x$  species representative for the in-situ number of active sites after ~100-200 h TOS as a function of the initial number of active sites before reaction as determined by dynamic CO adsorption for all 5 catalysts at 215, 225 & 235°C.

Using these carbon containing intermediates and assuming that the propagation and termination reactions are sufficiently fast to neglect the coverage of hydrocarbons, the total number of active sites can be calculated. Figure 4 plots the total number of active sites from SSITKA versus the initial number of active sites determined by dynamic CO adsorption for the 5 catalyst samples at the three reaction temperatures. A decrease between 5 - 35% of the initial number of sites is observed and in line with the deactivation of the catalysts. The deactivation process seems similar to all samples, indicated by the linear correlation in Figure 4 for all samples. This approach thus allows an *in-situ* determination of the number of active sites.

Although similar reaction conditions and the same amount of catalyst have been applied for the 5 samples during the first part of the test (~150 h), differences in CO conversions are observed.

Before these differences can be attributed to differences in cobalt phase orientation or particle size, the activity data has to be normalized with respect to the number of cobalt surface sites, which are different for the 5 samples. This is further complicated by the fact that the activity decreases with TOS due to a decrease in the number of active sites. Generally in the literature to compare catalyst performances normalized with respect to the number of active sites, TOF's are used. TOF is the reaction rate per active site and thus depends on the reaction conditions, in our case specifically the level of conversion. A better comparison of the different samples is by comparing the rate constants. Therefore the CO conversion data have been modeled with respect to a simple kinetic rate equation. The following rate equation, in reparametrized form, for the consumption of CO, originally proposed by Sarup and Wojciechowski [25] and often encountered in the literature, has been used:

$$-r_{CO} = \frac{N_s k' \exp\left(\frac{-E_{app}}{R} \left(\frac{1}{T} - \frac{1}{493}\right)\right) P_{CO}^{0.5} P_{H_2}^{0.5}}{(1 + b P_{CO}^{0.5})^2}$$

where,  $N_s$  is the number of active sites,  $k'$  a reparametrized pre-exponential factor,  $E_{app}$  the apparent activation energy,  $R$  the gas constant. The constant  $b$  in the denominator was assumed to be independent of the temperature between 205-235°C. The value for the number of active sites as determined by SSITKA  $^{12}CO/H_2 \Rightarrow ^{13}CO/H_2$  switches has been used for  $N_s$  in the above rate equation. This corresponds to the number of active Co surface sites during the run, which are lower than the initial number of active sites. The use of the initial number of active sites would have induced a systematic error in the value of  $k'$  for all samples.

**Table 2.** Parameter estimates and their 95% confidence intervals for a rate equation (1). The data for each catalyst sample are fitted to the rate equation separately.

sample	$k'$ (Pa <sup>-1</sup> s <sup>-1</sup> )	$E_{app}$ (kJ/mol)	$b$ (Pa <sup>-0.5</sup> ) <sup>[a]</sup>
CoPt/Al <sub>2</sub> O <sub>3</sub> - 6nm	1.03±0.11 10 <sup>-5</sup>	96 ± 15	0.025
CoPt/Al <sub>2</sub> O <sub>3</sub> - 10nm	1.18±0.08 10 <sup>-5</sup>	95 ± 9	0.025
CoPt/Al <sub>2</sub> O <sub>3</sub> - 15nm	1.32±0.34 10 <sup>-5</sup>	95 ± 26	0.025
Co/Al <sub>2</sub> O <sub>3</sub> - 10nm (fcc)	1.26±0.09 10 <sup>-5</sup>	98 ± 8	0.025
Co/Al <sub>2</sub> O <sub>3</sub> - 10nm (hcp)	1.32±0.15 10 <sup>-5</sup>	89 ± 10	0.025

[a] parameter fixed during regression analysis....

A set of intrinsic kinetic data at different conditions per sample was available to estimate the parameters of the above rate equation (43 data points for all 5 samples). The value for parameter  $b$  was fixed at a value of 0.025 Pa<sup>-0.5</sup> after an initial regression analysis of the all the data. This value is in the range of values reported in the literature [26]. Table 2 lists the parameter estimates,  $k'$  and  $E_{app}$ , obtained by regression analysis of the data

of each catalyst sample separately. Table 2 also reports the 95% confidence intervals of the estimated parameters. Due to the small number of data points this interval is sometimes rather large. In all cases a very good fit of the experimental conversion was achieved without any systematic deviations.

**Table 3.** Parameter estimates in rate equation (1) with their 95% confidence intervals by regression analysis of all 5 samples simultaneously (43 data points).

Parameter	estimated value with 95% confidence interval
$k'$ (Pa <sup>-1</sup> s <sup>-1</sup> )	1.46±0.59 10 <sup>-5</sup>
$E_{app}$ (kJ/mol)	97.6 ± 4
$b$ (Pa <sup>-0.5</sup> )	2.73 ± 0.68 10 <sup>-2</sup>

Even though for each sample the kinetic data set was small, statistically correct parameter estimates were obtained. The activation energy ranged from 89 to 98 kJ/mol. Actually, all these values fall within one standard deviation (5 kJ/mol). The reparametrized pre-exponential factor,  $k'$ , is very similar too, for all 5 samples. No trends with respect of the cobalt structure (fcc vs hcp, Pt promotor, particle size) can be discerned.

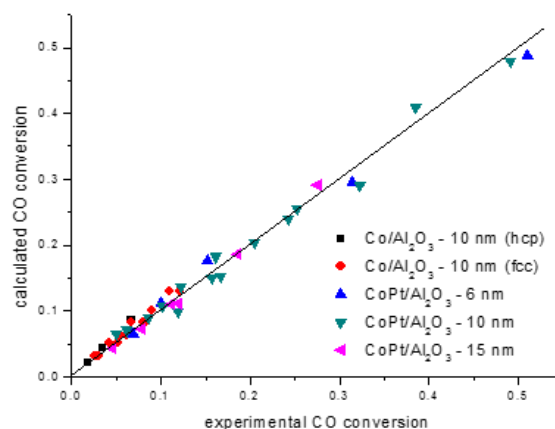


**Figure 5.** Parity plot for the CO conversion of all 5 Co/Al<sub>2</sub>O<sub>3</sub> catalysts fitted simultaneously by rate equation (1).

Thus the kinetics over the 5 samples suggest that they can be described by a single set of parameters with rate equation (1). Therefore the data were refitted by a regression analysis of all the data simultaneously. This time all three parameters,  $k'$ ,  $E_{app}$  and  $b$  were estimated.  $N_s$  still corresponds to the number of active sites after 150 TOS, different for each sample and determined from the

SSITKA data. Figure 5 shows the parity plot. An adequate fit was obtained for all data. Table 3 lists the values of the parameter estimates. A strong correlation coefficient between  $k'$  and  $b$  of 0.995 was found, which explains the rather large 95% confidence interval on  $k'$  and  $b$ . The value of 97.6 kJ/mol for the apparent activation energy is within the range reported in the literature for FTS over cobalt based catalysts [27].

Thus the difference in conversion levels observed in Figure 1 is only due to the differences in the number of active sites. None of it can be attributed to a difference in particle size, phase orientation (fcc or hcp) or promoting effect. The Pt promoted samples clearly outperform the non-promoted ones. The determination of the number of active sites before and during reaction shows that this is due to the higher number of reduced cobalt surface sites in the promoted samples than the not promoted ones. The fcc sample lead to higher CO conversion levels than over the hcp sample. Again this difference can be attributed fully to the different number of active sites as the data over both samples are described by the same rate equation.

Rane et al. [12] did not observe a Co particle effect either on the FTS activity for a large series of different alumina's ( $\alpha, \theta, \delta, \gamma$ ) supported catalysts. The catalyst preparation and loading are comparable to the ones used in this study. The catalysts were tested at 210°C and 20 bars and were kept 100 h on stream. Fischer et al. [14], on the other hand, did find an increasing TOF with increasing Co particle size for alumina supported catalysts. However, the catalyst preparation and loading were very different than used here. The catalysts were tested at 190°C and 9.9 bars and were kept 24 h on stream. The particle size activity dependence was much more pronounced for a fresh sample than after 24 h on stream. This is an important difference with the current study where the data are analyzed at 150 h TOS. It is likely after 150 h TOS that the smallest particles were impacted the most by the deactivation and have probably sintered, oxidized or have formed cobalt/aluminates phases. In this study, however, this loss of active phase is accounted for by using the *in-situ* number of active sites.

Contrary to our results, both Ducreux et al. [28] and Karaca et al. [29] reported higher activities for the hcp compared to the fcc phase of alumina supported cobalt catalysts, but they did not report any TOF's. Chu et al. [30] attributed the increased activity of the platinum promoter cobalt catalyst to an increased number of exposed cobalt sites, in agreement with the results in this study. The fact that the steady-state kinetics are identical for all 5 catalysts is supported also by the transient data. The surface lifetime of the intermediates leading to methane and the surface coverages of adsorbed CO, the monomeric carbon species and the  $\text{CH}_x$  species all show the same trends with conversion, irrespective of the catalyst sample.

Consequently, for the design of industrial FTS catalysts with high activity, the initial state of the cobalt particles seems to be less important than the studies over model supports imply. Rather, the number of active reduced cobalt sites should be maximized, which in this study was for the 6 nm CoPt/Al<sub>2</sub>O<sub>3</sub> sample.

To summarize, the steady-state rate of CO conversion over all 5 Co/Al<sub>2</sub>O<sub>3</sub> samples can be described by the following rate equation:

$$-r_{\text{CO}} = \frac{N_s 3.2 \cdot 10^5 \exp\left(\frac{-97600}{RT}\right) P_{\text{CO}}^{0.5} P_{\text{H}_2}^{0.5}}{(1 + 0.0273 P_{\text{CO}}^{0.5})^2} \text{ (mol kg}_{\text{cat}}^{-1} \text{ s}^{-1})$$

or in terms of TOF:

$$\text{TOF} = \frac{3.2 \cdot 10^5 \exp\left(\frac{-97600}{RT}\right) P_{\text{CO}}^{0.5} P_{\text{H}_2}^{0.5}}{(1 + 0.0273 P_{\text{CO}}^{0.5})^2} \text{ (s}^{-1})$$

At 220°C and  $\text{H}_2/\text{CO}=2$ ,  $P=1$  bar, a TOF of  $1.9 \cdot 10^{-2} \text{ s}^{-1}$  is calculated. This is well within the range of  $0.2 - 2.5 \cdot 10^{-2} \text{ s}^{-1}$  reported in the literature under similar conditions over different Co based catalysts [7, 9, 19, 31] and corresponds even better with TOF's reported for Co particles larger than 10 nm.

### Selectivity

Figure 6 shows the product distribution grouped as methane, C<sub>2</sub>-C<sub>4</sub> and C<sub>5</sub>+ selectivity as a function of the CO conversion for

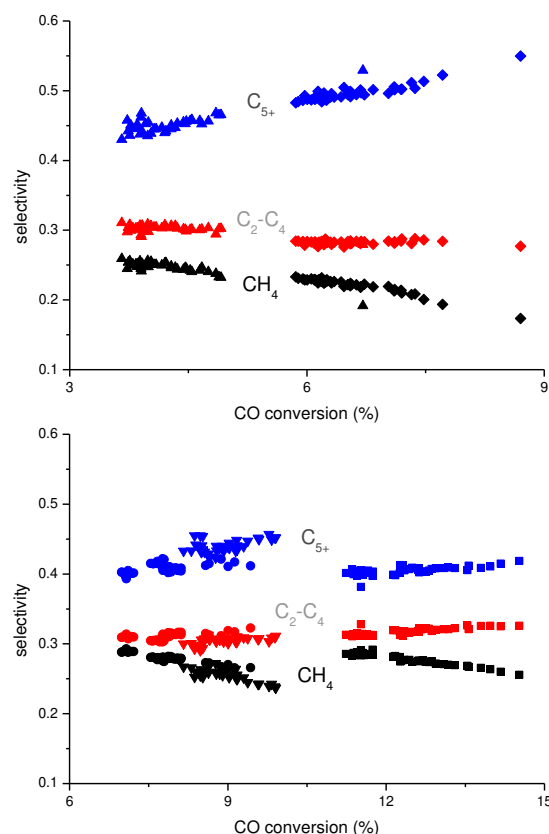


**Figure 6.** Lumped selectivity C<sub>1</sub>, C<sub>2</sub>-C<sub>4</sub> and C<sub>5</sub>+ versus CO conversion ( $\text{H}_2/\text{CO}=2$ , 30 Nml/min; Ar, 20 Nml/min;  $P=1.7$  bar) and constant temperature (Top graph 220°C). ▲: hcp Co/Al<sub>2</sub>O<sub>3</sub> 10 nm; ◆: fcc Co/Al<sub>2</sub>O<sub>3</sub> 10 nm; (Bottom graph 225°C) ●: CoPt/Al<sub>2</sub>O<sub>3</sub> 15 nm; ▼: CoPt/Al<sub>2</sub>O<sub>3</sub> 10 nm; ■: CoPt/Al<sub>2</sub>O<sub>3</sub> 6 nm.

the 5 catalyst samples. Clear trends as a function of the CO conversion emerge from these data sets, irrespective of the nature of the sample. Like the activity, the selectivity depends on the conversion level. With increasing conversion the  $C_{5+}$  selectivity increases with a simultaneous decrease of both the methane and  $C_2$ - $C_4$  selectivity. Similar trends as a function of the conversion were observed at different temperatures although the selectivity depended strongly on the temperature. This effect has already been reported [32].

All selectivity data at all temperatures can be summarized by plotting the  $C_1$  and  $C_2$ - $C_4$  selectivity versus the  $C_{5+}$  selectivity, as shown in Figure 7. Similar trends were already reported in the literature at higher pressure [33].

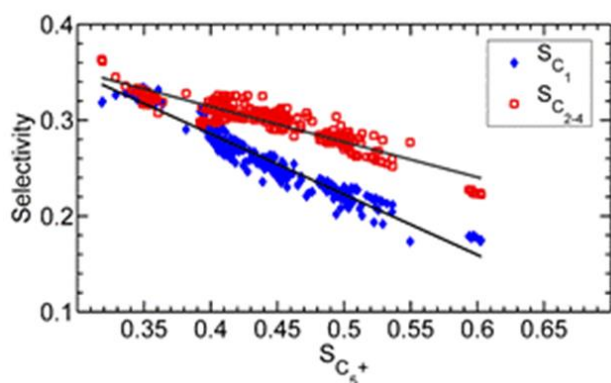


**Figure 7.** Lumped selectivity  $C_1$ ,  $C_2$ - $C_4$  versus  $C_{5+}$  selectivity for the 5 catalyst samples at all temperatures (205-235 °C).

## Conclusions

Five alumina supported cobalt catalysts with different particle size and structure were synthesized and tested during long-term runs for FTS. SSITKA experiments carried out during these runs, allowed through the summation of all surface intermediates estimating the number of active sites during reaction. A simple kinetic rate equation based on the *in-situ* number of active sites describes adequately the CO conversion over 5 catalyst samples. Thus the difference in the catalytic performance cannot be attributed to a difference in particle size, phase orientation (fcc or hcp) or Pt promoting effect, but instead only to the number of reduced cobalt atoms exposed, i.e. the number of active sites for CO adsorption and activation, during reaction. Similarly, the selectivity depends on the CO conversion level and temperature, but not on the catalyst structure.

To design industrial alumina supported FTS catalysts with high activity, the number of reduced cobalt sites during reaction should be maximized, without any constraints on the initial cobalt particle size or phase orientation.

## Experimental Section

### Catalysts

Three cobalt supported on alumina catalysts promoted by platinum were prepared, aiming for three different particles sizes. A fourth cobalt supported on alumina catalyst without Pt promoter was also prepared and part of this sample was further treated to change the cobalt crystal orientation from mainly face-centered cubic phase (fcc) to the cobalt hexagonal close-packed phase (hcp). Thus in total 5 catalysts were used in this study.

Cobalt catalysts were prepared by incipient wetness impregnation of Puralox  $\gamma$ -alumina SCCa (Sasol GmbH, 80 micron grain size, BET surface area of 166 m<sup>2</sup>/g) with a nitrate cobalt solution. Hexa-hydrate nitrate cobalt salt (Co (NO<sub>3</sub>)<sub>2</sub>, 6H<sub>2</sub>O) was dissolved in a mixture of 90% distilled water and 10% ethylene glycol to obtain the impregnation solution as described in the literature [19] with a cobalt concentration of 13.4 wt. %. Ethylene glycol was used to increase the cobalt dispersion on the surface. After 2 h the catalyst was left to dry overnight under air at 85 °C and was then calcined in a tubular fixed bed reactor for 4 h with either a heating ramp of 1 °C/min and an air flow of 1 NL/h/g<sub>cat</sub> or a heating ramp of 5 °C/min and an air flow of 0.5 NL/h/g<sub>cat</sub>. This impregnation process was repeated twice to reach the target cobalt loading of approximately 13 wt. %. In case of Pt promotion, Pt precursor (tetraammineplatinum hydroxide) was added to the impregnation solution (9.3 wt% Pt). Targeted metal loading of Pt was 500 ppm.

The catalysts underwent different activation processes as described in more detail in [23]. Direct reduction consisted of exposing the sample to a flow of pure hydrogen during the temperature ramp (from room temperature with 2 °C/min up to 500 °C) and during the temperature dwell fixed at 500 °C for 16 h. This leads to cobalt particles that consist largely of a face-centered cubic phase. An alternative activation step consisted of exposing the catalysts to a flow of pure carbon monoxide and then to a flow of hydrogen at 230 °C after the direct reduction step. This activation process involves a carbidisation-decarbidity cycle and leads to a largely cobalt hexagonal close-packed phase [23].

Carbon monoxide chemisorption was carried out at room temperature by the dynamic sorption technique described by Couble and Bianchi [34].

### Ex situ characterization techniques

Before activation, the catalysts were characterized by a wide range of *ex-situ* techniques. The BET surfaces areas were measured by nitrogen physisorption at 77 K using an ASAP 2420. The pore size diameter of the catalysts was measured by mercury porosimetry. Morphological analysis on a cross section were performed using a Zeiss supra 40 SEM microscope. Cobalt repartition was observed with the retrodiffused electron detector. Cobalt and platinum loading was measured by wavelength dispersive X-Ray Fluorescence with a Thermo Advant'X system (Platinum content is only estimated with a +/- 20% error according to the low loading used and is slightly underestimated). XRD measurements were carried out on a PANalytical diffractometer. The most intense Co<sub>3</sub>O<sub>4</sub> line (311) was used to calculate the average Co<sub>3</sub>O<sub>4</sub> particle size with the Scherrer equation (K=1). Dark field transmission electron microscopy was used to establish the particle size distribution using 300-400 particles.

## Steady-state and transient catalyst testing

Catalyst testing for FT synthesis was carried out in a quartz plug flow reactor at 1.6 bar, 220°C or 225°C with a H<sub>2</sub>/CO ratio of 2 and about 200 - 300 hours of time on stream (TOS) to account for catalyst ageing. The reactor consisted of a 4 mm i.d. tube in which 300 mg of catalyst diluted in 300 mg of SiC powder was placed and further filled completely with SiC to avoid any dead volume. Three thermocouples were inserted inside the catalyst bed to monitor the temperature profile during reaction. The quartz reactor was inserted in a tubular oven that can achieve the reduction at 450°C with a temperature gradient lower than 10°C. At FTS conditions the temperature gradient is less than 3°C.

During the 200 - 300 hour run, several <sup>12</sup>CO→<sup>13</sup>CO SSITKA experiments were carried out. The reactor was fed with a mixture of 20 Nml/min H<sub>2</sub>, 10 Nml/min CO and 20 Nml/min Ar. Towards the end of the run, the reactor temperature was changed between 205 and 235°C, as well as the H<sub>2</sub>/CO ratio between 2 - 10, in order to establish a steady-state rate equation. The CO conversions during these tests ranged from 2 to 50%.

## Chemical analysis

The online analysis system was composed of two cryogenic GC/FID-TCD and GC/MS (HP 6890 equipped with PONA columns (100 m) for hydrocarbons separation) with 16 storage loops and a MS gas analyzer (Inficon, Compact Process monitor). The combination of these techniques allowed monitoring product distribution (paraffins, α- and β-olefins and isomers) and determining the isotopic composition of a large range of products during the transient (paraffin and α-olefins from C<sub>1</sub> to C<sub>5</sub>). Quantitative analysis is made from C<sub>1</sub> to C<sub>13</sub> with a good resolution for every isomer up to C<sub>6</sub>. Because of the relatively low operating pressure (<3 bar) and low alpha values (<0.7) no heavy products were accumulated and products higher than C<sub>13</sub> were detected but were not quantifiable. The standard deviation of the outlet CO concentration of the TCD is approximately 5% and does not allow a good accuracy at low CO conversion. The CO conversion was determined by using the method developed by Bell *et al.* [35] for low conversion (X<sub>CO</sub><10%), which considers the summation of all hydrocarbons based on the FID detector response and provides the best accuracy for X<sub>CO</sub>.

$$\chi_{CO} = \frac{Q_{out} \sum_{i=1}^n \nu_i C_i}{Q_{in} C_{CO}^0}$$

In this expression, Q<sub>out</sub> is the volumetric flow at the reactor outlet during reaction, Q<sub>in</sub> is the volumetric flow at the reactor inlet during reaction, ν<sub>i</sub> is the stoichiometric factor, C<sub>i</sub> is the concentration of hydrocarbon with carbon number i, and C<sub>CO</sub><sup>0</sup> is the concentration of CO at the reactor inlet.

The product selectivity was calculated using

$$S_{C_j-C_k} (\%) = \frac{\sum_{i=j}^k \nu_i C_i}{\sum_{i=1}^n \nu_i C_i}$$

## SSITKA data treatment

From the raw integration of the normalized response, the surface lifetime of the species are obtained after correcting the average residence time by the inert tracer. Kr represent the hold-up of the reactor system. The

residence time τ<sub>i,r</sub> was obtained from step-up transients with the following expressions respectively:

$$\tau_{i,r} = \int_0^{\infty} F_i(t)$$

The surface lifetimes τ<sub>i,s</sub> were calculated by:

$$\tau_{CO,s} = \tau_{CO,r} - \tau_{Kr,r}$$

$$\tau_{CH_4,s} = \tau_{CH_4,r} - \frac{1}{2} \tau_{CO,s} - \tau_{Kr,r}$$

In the last equation, the surface lifetime of methane is corrected for the chromatographic effect of CO in a plug-flow reactor, as is custom in the literature [36]. The amount of intermediates leading to methane is calculated from τ<sub>CH<sub>4</sub>,s</sub> and the outlet flow of methane, :

$$N_{CH_4,s} = \tau_{CH_4,s} \cdot F_{CH_4}$$

## Modeling

By using the well-known criteria [37], the absence of heat and mass transfer limitations were checked. This allowed to use a rather simple model that only takes into account the chemical kinetics. The experimental fixed bed reactor was modeled as a one-dimensional pseudo-homogeneous isothermal plug-flow reactor. The stoichiometric coefficient for the hydrogen consumption has been fixed at 2. This leads to the two following differential equations:

$$\frac{dF_{CO}}{dW} = -r_{CO}$$

$$\frac{dF_{H_2}}{dW} = -2r_{CO}$$

Where F<sub>CO</sub> and F<sub>H<sub>2</sub></sub> are the molar flow rates of carbon monoxide and hydrogen (mol/s), respectively, W the catalyst mass (kg) and r<sub>CO</sub> the CO consumption rate (mol/s/kg<sub>cat</sub>). These ordinary first-order differential equations were numerically integrated using the ODEPACK library [38]. The non-linear single response least-square regression analysis has been performed by a Levenberg-Marquardt minimization algorithm [39,40]. The experimental and calculated CO conversion were used to calculate the objective function. After regression analysis several statistical tests were performed.

## Acknowledgements

IFP Energies nouvelles is gratefully acknowledged for supporting this study.

**Keywords:** Particle size • SSITKA • Turnover Frequency • C5+ selectivity • syngas

- [1]. <http://www.ifpenergiesnouvelles.com/News/Press-releases/Inauguration-of-the-BioTfuel-project-demonstrator-in-Dunkirk-2nd-generation-biodiesel-and-biokerosene-production-up-and-running>, verified 05/01/2017.
- [2]. C. Reuel, C.H. Bartholomew, *J. Catal.* **1984**, *85*, 78-88.
- [3]. B.G. Johnson, C.H. Bartholomew, D.W. Goodman, *J. Catal.* **1991**, *128*, 231-247.
- [4]. S.W. Ho, M. Houalla, D.M. Hercules, *J. Phys. Chem.* **1990**, *94*, 6396 – 6399.
- [5]. E. Iglesia, S.L. Soled, R.A. Fiato, *J. Catal.* **1992**, *137*, 212-224.
- [6]. A. Barbier, A. Tuel, I. Arcon, A. Kodre, G.A. Martin, *J. Catal.* **2001**, *200*, 106–116.
- [7]. G. L. Bezemer, J.H. Bitter, H.P.C.E. Kuipers, H. Oosterbeek, J.E. Holeywijn, X. Xu, F. Kapteijn, A.J. van Dillen, K.P. de Jong, *J. Am. Chem. Soc.*, **2006**, *128(12)*, 3956-3964.
- [8]. O. Borg, P.D.C. Dietzel, A.I. Spjelkavik, E.Z. Tveten, J.C. Walmsley, S. Diplas, S. Eri, A. Holmen, E. Rytter, *J. Catal.* **2008**, *259*, 161–164.
- [9]. J. Den Breejen, P. B. Radstake, G. L. Bezemer, J. H. Bitter, V. Frøseth, A. Holmen, and K. P. de Jong, *J. Am. Chem. Soc.* **2009**, *22*, 7197–7203.
- [10]. A.Y. Khodakov, *Catal. Today* **2009**, *144*, 251–257.
- [11]. S. Rane, Ø. Borg, J. Yang, E. Rytter, A. Holmen, *Appl. Catal. A: Gen.* **2010**, *388*, 160-167.
- [12]. S. Rane, Ø. Borg, E. Rytter, A. Holmen, *Appl. Catal. A: Gen.* **2012**, *437–438*, 10–17.
- [13]. Z. Wang, S. Skiles, F. Yang, Z. Yan, D.W. Goodman, *Catal. Today* **2012**, *181*, 75–81.
- [14]. N. Fischer, E. van Steen, M. Claeys, *J. Catal.* **2013**, *299*, 67–80.
- [15]. N. Fischer, B. Clapham, T. Feltes, M. Claeys, *ACS Catal.* **2015**, *5*, 113–121.
- [16]. J. Yang, V. Froseth, D. Chen, A. Holmen, *Surf. Sci.* **2016**, *648*, 67-73.
- [17]. H. Schulz, Z. Nie, F. Ousmanov, *Catal. Today* **2002**, *71*, 351-360.
- [18]. D. Kistamurthy, A. M. Saib, D. J. Moodley, J. W. Niemantsverdriet, C. J. Weststrate, *J. Catal.* **2015**, *328*, 123-129.
- [19]. A. Carvalho, V. Ordonsky, Y. Luo, M. Marinova, A.R. Muniz, N.R. Marcilio, A.Y. Khodakov, *J. Catal.*, **2016**, *344*, 669–679.
- [20]. G. Lente, *ACS Catal.*, **2013**, *3*, 381–382.
- [21]. H. A. J. Van Dijk, J. H. B. J. Hoebink, and J. C. Schouten, *Top. Catal.* **2003**, *26* (1–4), 163–171.
- [22]. A. Jean-Marie, PhD Thesis Lille University, **2010**.
- [23]. L. Braconnier, E. Landrison, I. Cléménçon, C. Legens, F. Diehl, Y. Schuurman, *Catal. Today*, **2013**, *215*, 18–23.
- [24]. E. Rebmann, P. Fongarland, V. Lecocq, F. Diehl, Y. Schuurman, *Cat. Today* **2016**, *275*, 20-26.
- [25]. B. Sarup, B.W. Wojciechowski, *Can. J. Chem. Eng.* 1989, *67*, 62-74.
- [26]. P. Azadi, G. Brownbridge, I. Kemp, S. Mosbach, J. S. Dennis, M. Kraft, *ChemCatChem* **2015**, *7*, 137-143.
- [27]. C. H. Bartholomew and R. J. Farrauto, "Fundamentals of Industrial Catalytic Processes," 2<sup>nd</sup> Ed., Wiley, 2011
- [28]. O. Ducreux, B. Rebours, J. Lynch, and D. Bazin, *Oil & Gas Sci. & Techn.* **2009** *64* (1), 49–62.
- [29]. H. Karaca, O. V. Safonova, S. Chambrey, P. Fongarland, P. Roussel, A. Griboval-Constant, M. Lacroix, and A. Y. Khodakov, *J. Catal.* **2011**, *277* (1), 14–26.
- [30]. W. Chu, P.A. Chernavskii, L. Gengembre, G.A. Pankina, P. Fongarland, A.Y. Khodakov, *J. Catal.* **2007**, *252*, 215–230.
- [31]. Kogelbauer
- [32]. A. Tavasoli, A. Khodadadi, Y. Mortazavi, K. Sadaghiani, and M. G. Ahangari, *Fuel Process. Technol.*, **2006**, *87* (7), 641–647.
- [33]. S. Lögdberg, M. Luaidi, S. Järs, J.C. Walmsley, E.A. Blekkan, E. Rytter, and A. Holmen, *J. Catal.* **2010**, *274* (1), 84–98.
- [34]. J. Couble and D. Bianchi, *Appl. Catal. A Gen.* **2012**, *445–446*, 1–13.
- [35]. A. Dinse, M. Aigner, M. Ulbrich, G. R. Johnson, A. T. Bell, *J. Catal.* **2012**, *288*, 104–114.
- [36]. S.L. Shannon, J.G. Goodwin, *Chem. Rev.* **1995**, *95*, 677–695.
- [37]. R.J. Berger, E.H. Stitt, G.B. Marin, F. Kapteijn, J.A. Moulijn, *CatTech* **2001**, *5*, 36-60.
- [38]. Hindmarsh A.C. ODEPACK, A Systematized Collection of ODE Solvers. Amsterdam: Elsevier, 1983.
- [39]. Levenberg K. Q. *Appl. Math.* 1944, *11*, 164-168.
- [40]. Marquardt DW. *J. Soc. Ind. Appl. Math.* **1963**, *11*, 431-441.